International Journal on Advanced Science Engineering Information Technology

Vol.14 (2024) No. 3
ISSN: 2088-5334

# Numerical Study of Wind Flow Behavior Around High-Rise Buildings Using Computational Fluid Dynamics (CFD)

Arga Yudhistira [a], Prasanti Widyasih Sarli [a,*], Syarie Fatunnisa [b], Alfredo Fikri Akbar [a], Yongky Sanjaya [a], Doni Priambodo [a]

[a] *Faculty of Civil and Environmental Engineering, Institut Teknologi Bandung, Jl. Ganesa No. 10 Lb, Bandung, Indonesia*
[b] *Laboratory for Aerodynamics, Aeroelastic, and Aeroacoustics Technology, National Research and Innovation Agency, South Tangerang, 15314, Banten, Indonesia*

*Corresponding author: [*]pw.sarli@itb.ac.id*

***Abstract*—The development of civil construction technology in Indonesia is progressing along with the rise in high-rise building construction. The emergence of high-rise buildings has altered wind flow characteristics, leading to phenomena that can directly impact surrounding structures. One of the observable phenomena is the wind speed amplification caused by the narrowing of the wind flow section, known as the Venturi effect. This study aims to compare the outcomes of two Computational Fluid Dynamics (CFD) methods—Reynolds-Averaged Navier-Stokes (RANS) and Large Eddy Simulation (LES)—against experimental results. The study employs a model of four buildings of similar height and symmetrical positioning, with a 72 mm passage width, to verify numerical simulations against experimental data. The RANS method yields a maximum wind speed amplification of 14.9% along the passage's centerline, which remains below the experimental prediction of 25.5% in Zone A. Conversely, the LES results show a higher wind speed amplification, reaching 40.2%, surpassing the experimental findings. Nevertheless, LES identifies a similar location for wind speed amplification observed in Zone A. Additionally, CFD simulations were conducted to analyze the effects of passage width, revealing that a passage width of 54 mm produces the highest wind speed amplification, with a ratio value of passage width to building influence scale (L/S) of 0.481. Further research on building model scale may be necessary to verify CFD accuracy compared to the actual scale. However, such simulations demand exceedingly high computational resources with current technology.**

***Keywords*— Wind load; lateral load amplification; wind load amplification; venturi effect; CFD; RANS; LES.**

*Manuscript received 24 Feb. 2023; revised 5 Oct. 2023; accepted 12 Mar. 2024. Date of publication 30 Jun. 2024.*


## I. INTRODUCTION

Wind plays a significant role in causing damage to construction projects in Indonesia. National Agency for Disaster Management (BNPB), 121 reported cases of wind-related damage in West Java occurred between 2012 and 2015 [1]. The wind is consistently the second or third source of residential damages, which shows that there us a need to understand the nature of wind as a hazard [2]. This underscores the importance of considering wind loading in structural design. Additionally, the construction of high-rise buildings in urban areas can cause wind-induced interference effects that may result in a substantial increase or reduction in wind forces on the buildings constructed in groups [3]. One of the phenomena where the windspeed increase caused by the change in the section is called venturi effect. The venturi effect occurs when wind passes through a narrowed area, such as between high-rise buildings, resulting in decreased static pressure and increased speed. Understanding wind behavior around buildings is a complex task, with previous studies addressing it through experimental or numerical methods [4].

In 1986, Stathopoulos and Storms [5] conducted wind tunnel experiments to investigate changes in wind speed between structures with varying passage widths and angles of attack. The highest wind speed amplification was observed at the entrance of the passage. Similarly, Blocken et al. [6] conducted experiments to study wind flow in a passage between two long buildings that were orthogonal to each other, forming either a converging or diverging passage. The observed parameters included passage width, building height, and angle of attack. Observations were made at the centerline of the enactment at the Pedestrian Wind Level (PWL). The results indicated that wind speed amplification in the diverging passage was generally more significant than in the

converging passage, although this was not always the case. Both studies focused on observing wind flow behavior only at the centerline of the passage between buildings due to using hotwire anemometers, which are relatively expensive and can only be deployed in limited numbers. As a result, these experimental setups could not capture amplification factors beyond the centerline.

Subsequently, Liu et al. [7] employed Particle Image Velocimetry (PIV) in their wind tunnel experiments to establish a comprehensive database for validating Computational Fluid Dynamics (CFD) analysis, specifically Large Eddy Simulation (LES). PIV is a non-intrusive optical technique for measuring fluid velocities in two or three dimensions. In PIV, minuscule particles, such as tracer particles, are introduced into the fluid flow and illuminated with a laser. The movement of these particles is then captured using a camera, allowing for the calculation of fluid velocity based on the displacement of the particles between successive images. Although PIV results still has its own uncertainty and validation needs to be done to sort some areas with high uncertainty [8]. PIV technology is a promising alternative for observing wind flow around objects, offering more detailed information than hotwire anemometry.

Some approach using Computational Fluid Dynamics (CFD) has been utilized since the 1960s, coinciding with the emergence of computer technology research. Reynold Averaged Navier-Stokes (RANS) and Large Eddy Simulation (LES) are two commonly employed CFD methods. Both methods are expected to simulate behavioral changes in wind flow accurately. Consequently, they enable the proposal of wind load recommendations for structures to minimize the potential for wind-induced damage.

Blocken et al. [9] employed Computational Fluid Dynamics (CFD) to examine the impact of passage width between two parallel buildings on wind speed amplification. This study utilized a ratio, denoted as w/S, to characterize the building formation. Here, 'w' represents the passage width, and 'S' represents the building influence scale, defined as the square cube of the building's width multiplied by the square of its length. The findings were utilized to categorize wind flow behavior into three types as follows:

- Resistance flow ($w/S < 0.125$): a flow through a narrow passage where resistance is dominant).
- Isolated flow ($w/S > 1.25$): a flow through a wide passage where there is no interaction between two corner streams and no speed amplification.
- Interaction flow ($0.125 < w/S < 1.25$): a flow with an interaction between the two corner streams, forming a wide single passage jet.

The highest wind amplification may happen at interaction flow. Although Blocken's results provide valuable insights, it's important to note that they were obtained using CFD only.

Research conducted by Sanjaya et al. [10] utilized RANS to examine the influence of passage width on wind flow between four symmetrical high-rise buildings. Two different passage widths were investigated, with the first model resulting in interaction flow and the second resulting in isolated flow. Sanjaya concluded that interaction flow could lead to up to 22% wind speed amplification, while isolated flow could result in up to 6%. However, it's important to note that the data was only collected at the center of the passage. Another study conducted by Priambodo et al. [11] also used RANS to investigate wind flow in a street canyon comprising a cluster of four simplified symmetrical high-rise buildings with angles of attack of 0°, 30°, and 45°. The results indicated that wind speed amplification occurred only in models with an angle of attack of 0°. A deficient wind speed region was observed in the cross area of the models with angles of attack of 30° and 45°. More complex building clusters increased vortexes and turbulence in the cross area, decreasing wind speed [12].

The studies mentioned earlier primarily utilized the RANS method, which typically captures larger-scale turbulent structures and may not be suitable for simulating complex flows. On the other hand, LES can capture both large and small turbulent structures in the flow field, making it more appropriate for simulations of complex flows that require a higher level of detail. Liu et al. [7] employed LES to observe the flow around a low-rise building. The numerical results obtained through the LES approach exhibited good agreement with the Particle Image Velocimetry (PIV) experimental results. However, it's worth noting that the geometric shape of the building primarily influenced the predictive performance. The study found that the predictive performance was better for simpler geometries compared to more complex geometries for the other three models.

The studies above demonstrate that the venturi effect significantly influences wind speed amplification at Pedestrian Wind Levels (PWL) and small structure elevations. Wind speed amplification can reach up to 40% at the PWL level and 20% at small structure elevations. The highest wind speed amplification is likely to occur in the interaction flow, where the merging of corner streams plays a significant role in the emergence of turbulence in the passage between buildings.

Many studies investigating bluff bodies and building formations utilize CFD. One of the main advantages of CFD over wind tunnel testing is its capability to provide detailed data across the entire computational domain [13] [14] [15]. However, a major challenge associated with CFD results is their accuracy, particularly in predicting flow characteristics in the wake of objects. Therefore, CFD simulation results must undergo verification and validation, preferably using experimental data [16].

In this study, CFD simulations employing both RANS and LES will be conducted and validated with experimental results obtained from various locations within the passages of a high-rise building configuration. The objective is to determine the magnitude and location of the most significant wind speed amplification. Additionally, the impact of the venturi effect on wind load will be investigated.

## II. Materials and Methods

This study created several numerical models using two different CFD methods: RANS using OpenFOAM software and LES using Fluent software. These results were then compared with the experimental model. The flow chart of this study can be seen in Fig. 1.

### *A. Experimental Data*

The experiment used an Educational Small Wind Tunnel (ESWT), Particle Image Velocimetry (PIV) LaVision device

and its data acquisition system, and Python software for post-processing. The data was further processed into graphs of wind speed amplification for each zone, which will be compared with the numerical simulation results. The results were previously published and used for prior studies [10], [11], [12], but more comprehensive results are published here. The model is a grid of four typical building models arranged to form a passageway between the buildings. The configuration of the building used in the experiment can be seen in Fig. 2.

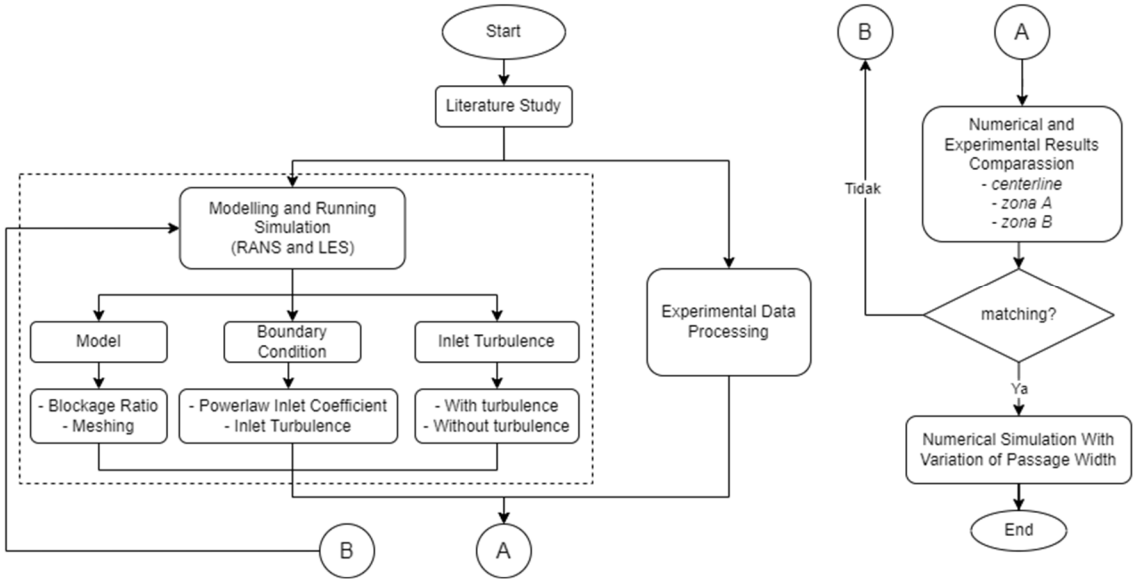


Fig. 1 Research Flowchart

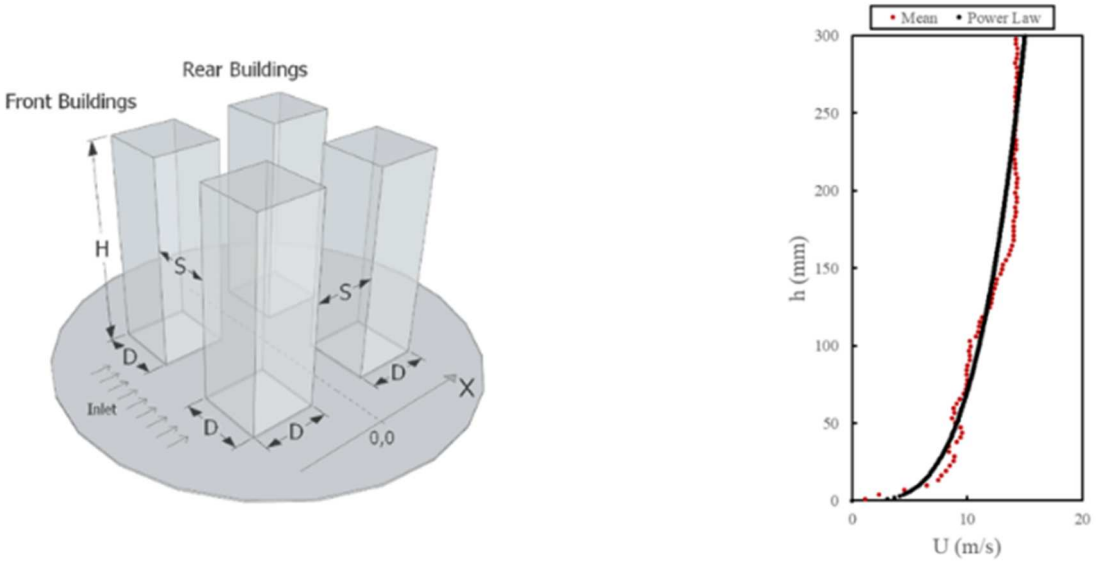


Fig. 2 Building model (left) and inlet profile (right)

TABLE I
MODEL PARAMETERS

| Parameters | Notation | Dimension in mm |
|---|---|---|
| Passage Width | $L$ | 72 |
| Building height | $H$ | 238 |
| Building width | D | 77 |

The building model was later tested by simulating the Atmospheric Boundary Layer (ABL) wind in urban areas [17]. The parameter value obtained to create the ABL wind profile in urban areas is the exponent α = 0.28 from the power-law function in which the measured incident mean wind speed profile resembled. The ABL wind profile follows the equation (1):

$$\frac{v}{v_{ref}} = \left(\frac{z}{z_{ref}}\right)^{\alpha} \quad (1)$$

$v$ wind speed at height z;
$v_{ref}$ reference wind speed (15 m/s);
$z$ height;
$z_{ref}$ reference height (100 mm);
$\alpha$ empirical value forming wind speed profile.

To obtain the value of α = 0.28, a set of turbulence generators was installed at the inlet of the tunnel test section. The reference wind speed value in this case was a freestream wind speed of 15 m/s along with turbulence intensity of 9.11% at an elevation of 100 mm. Fig 2. (right) represents the wind speed value against the measurement results' height in the wind tunnel test section from 10 data frames. The red data point is the mean of the 10 data frames. The reference wind speed at the wind tunnel was taken at an elevation of 100 mm, 10.281 m/s. In addition, for better comprehension, the following terms were used for areas that were in the direction of the wind, as illustrated in Fig.3:

- Upstream (US): the area before the building cluster.
- Front passage (FP): the area between the front buildings.
- Cross stream (CS): middle passage.
- Rear passage (RP): the area between the rear buildings.
- Downstream (DS): the area behind the building cluster.

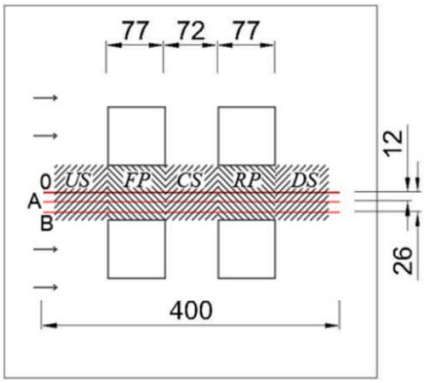


Fig. 3 Data Acquisition Location, dimensions are in mm

PIV data is taken by a high-speed camera of particle movements irradiated by a 2-dimensional laser sheet at an elevation of 100 mm. The data retrieval path was in several paths between buildings, as seen in Fig. 3. The measurement points of the obtained data included zone 0 (centerline), zone A, and zone B.

### *B. Numerical Setup*

In Steady State Simulation (RANS), the applied geometry and building position are the same as those in the experimentation. The difference is the size of the test domain, which will affect the blockage ratio and domain size. In his research using the same model, Sanjaya et al. studied the blockage ratio's effect on the simulation's accuracy compared to experimentation. The result was that the domain size of 2.2x1x4.05 with a blockage ratio of 1.67% showed a minimal error value for wind speed amplification at the centerline between buildings [10]. The geometry of the domain and the boundary conditions used can be seen in Fig. 4 and Table II.

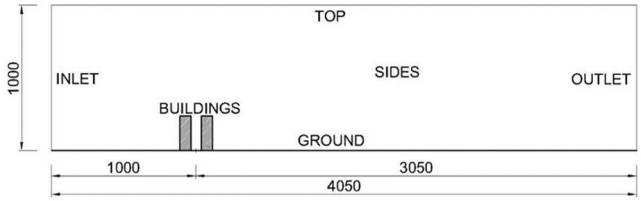


Fig. 4 Computational Domain for steady-state simulation (RANS) (in mm)

TABLE II
BOUNDARY CONDITION

| Parameter | Inlet | Outlet | Building | Ground | Top | Sides |
|---|---|---|---|---|---|---|
| **U** | Fixed profile power law | Pressure inlet-outlet velocity | noSlip | noSlip | noSlip | noSlip |
| **P** | Zero gradient | Fixed value (0,0,0) | Zero gradient | Zero gradient | Zero gradient | Zero gradient |
| **Nut** | Zero gradient | Zero gradient | Standard wall function | Standard wall function | Standard wall function | Standard wall function |
| **k** | Turbulent intensity inlet | Zero gradient | Standard wall function | Standard wall function | Standard wall function | Standard wall function |

To find out the most appropriate method to be implemented in steady-state simulation, the authors experimented by simulating the model with several steady-state models. In several past studies experimenting with several analysis parameters is likely done to found out which parameters suit the most with the experimental data [18] [19]. By using OpenFOAM software, several two-equation-based turbulence models were simulated, specifically as follows:

- Standard (SKE),
- Realizable (RKE),
- Renormalization Group (RNGKE).

Later, the results of the three turbulence models will be compared, and the results most suitable for experimentation will be used for further comparisons.

TABLE III
MESHING STRATEGY

| Area | Direction | Mesh Law | No of Partition |
|---|---|---|---|
| Passage between buildings | - Streamwise<br>- Cross-stream | - Varies<br>- Varies | Varies<br>Varies |
| Upstream | Streamwise | Half cosines | 36 |
| Downstream | Streamwise | Exponential | 68 |
| Side of the cluster | - Cross stream<br>- Vertical | - Exponential<br>- Full cosines | 24<br>36 |
| Freestream | Vertical | exponential | 24 |

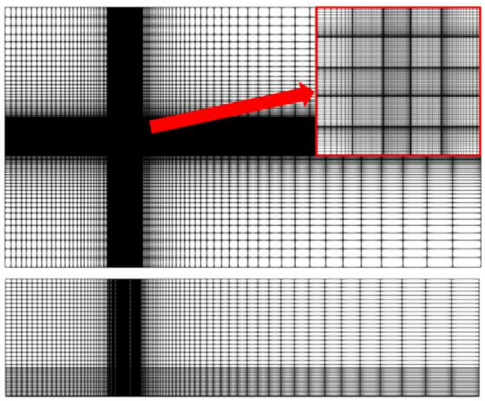

Fig. 5 Meshing Strategy. Top View (top) and Side View (bottom)

In LES modeling, achieving optimal results requires careful consideration of domain size, number of cells, mesh refinement, and simulation duration, especially within computational capacity constraints. Research conducted by Zidan et al. [20] on the significance of domain size in ensuring computational stability and solution convergence in LES simulations. There's a critical threshold where increasing domain size doesn't notably impact results, highlighting the importance of an efficient domain size to obtain optimal results without excessively long computation times. Conversely, using a much smaller domain size may significantly influence domain boundary conditions on the simulation outcomes.

Tominaga emphasized the significance of maintaining a blockage ratio of less than 3% when employing Computational Fluid Dynamics (CFD) to simulate wind flow between buildings [21]. This recommendation underscores the importance of ensuring that the obstruction caused by buildings in the computational domain remains within a certain threshold to capture the flow dynamics accurately. Furthermore, Tominaga suggested specific guidelines regarding the spatial arrangement within the computational domain. According to these guidelines, the distance between the upper boundary of the domain and the side boundaries should exceed 5 times the size of the buildings. In comparison, the distance between the buildings and the rear boundary of the domain should be more than 10 times the size of the buildings. These spatial parameters are crucial for preventing boundary effects from influencing the simulated flow patterns, ensuring that the results represent real-world conditions.

The most important attribute of simulations of Computational Fluid Dynamics (CFD) is meshing for domain and model [22]. In LES, the mesh size of the model is applied as a filter between the eddy solved (resolved scale) and the modeled (sub-grid scale), therefore the right meshing strategy should be done to obtain good results. Table III details the meshing strategy used, while Fig. 5 showcases an example of the detailed meshing utilized in LES modeling. This visual representation illustrates the spatial distribution of grid nodes and elements within the computational domain, highlighting the complexity of the mesh structure designed to capture the flow dynamics with high fidelity.

### C. *Numerical Experiment to observe passage width effect*

Multiple numerical simulations were conducted with varying passage widths to determine the optimal passage width capable of producing the highest wind speed amplification. The universal ratio introduced by Stathopoulos is used to characterize the wind flow behavior in the passage between buildings where L is the passage width, and S is the building influence scale, which in this building model obtained an *S* value of 112.16 [5]. Blocken et al. [9] stated that the flow type that produces the highest wind speed amplification is interaction flow. In this analysis, several numerical simulations representing interaction flow will be conducted with the variation of passage width 36, 54, 72, 96, and 120 mm, in which each passage width forms L/S values of 0.321, 0.481, 0.642, 0.856, and 1.070. The data retrieval will be done at the elevation of 100 mm, the reference elevation in the experimentation, and at the elevation of 30 mm, which is the wind elevation that would probably influence the small structure (12.6 meters on the actual scale).

## III. Results and Discussion

### A. *Experimental Data Processing*

Initially, the experimental data is processed to obtain valid data sets to be compared to the simulation results. One of the PIV's weaknesses is its sensitivity towards light obstruction, which can influence the measurement results. The red boxes from Fig. 6 represent the passage position. Meanwhile, the shaded area represents where the shadows fell, and the measurement results show anomalies. To maximize accuracy, the data obtained on the obstructed was eliminated. An example of data eliminated can be seen in Fig. 7, marked by the red circle.

In this research, the mean wind speed from each frame is used to analyze the wind flow behavior. The parameters used in the data processing are as follows:

- Wind speed in a specific location in which the building exists ($U$).
- Reference speed: wind speed in specific location in the absence of building ($U_{reff}$).
- Wind speed amplification: the ratio between the wind speed in which the building exists and the wind speed when there is no building ($U/U_{reff}$).

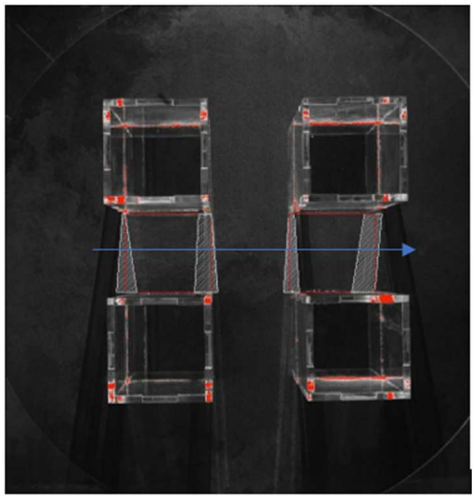

Fig. 6 Shadow Location and its effect on measurement results: PIV's frame

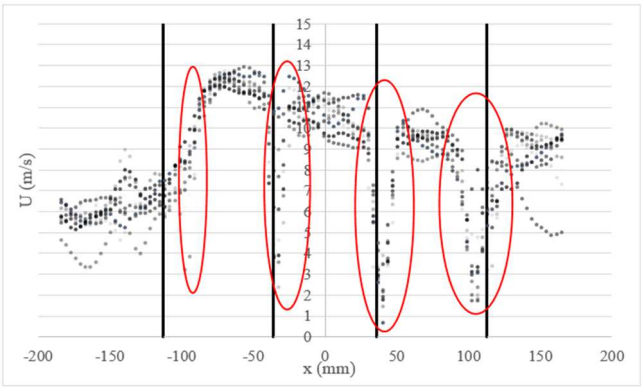


Fig. 7 Shadow Location and its effect on measurement results: streamwise wind speed data at the centerline

The wind speed amplification value from the streamwise direction data can be seen in Fig. 8-10. The ratio of wind speed at which buildings are accounted for, and the wind speed at which buildings are not accounted for are the parameters applied to describe the presence or absence of amplification of the occurred wind speed. The value defines an amplification of the wind speed at that position. The level of amplification experienced in each area differs on the value and location. The centerline zone's most significant wind speed amplification level is 20.1%, located in the middle of the front passage. Zone A's most considerable wind speed amplification level is 25.5%, in the middle of the front passage. Zone B's most significant wind speed amplification level is only 2.1% in the cross-stream. From the information above, it can be concluded that the most remarkable wind speed amplification does not occur in the centerline zone of the gap between buildings, as assumed by previous studies [2], [3], [5], [6], [7].

From Fig. 11, the wind flow pattern from each zone is typical. The average wind speed upstream is less, than $U_{reff}$ indicating blockage due to building clusters. The average wind speed increases as the wind flow enters the front passage, where the area of the cross-section of the wind flow starts to narrow. In the across-stream rear passage and downstream area the average wind speed tends to be less than or equal to $U_{reff}$, this phenomenon occurs in all zones.

### *B. Simulation Results: RANS vs LES*

From the simulation method and setup described in the methodology, numerical simulations were conducted to obtain the convergence of the numerical solutions of each steady-state and transient-state method. Furthermore, the wind speed amplification value of the two models will be compared.

Fig. 12-13 shows the mean wind speed contour at the top section at 100 mm height as the result of numerical simulation using Fluent software. The main observed difference is that LES can simulate turbulence at the rear side of the building's wake, which is not apparent on the RANS. Moreover, in LES, the wind speed pattern observed between the passage can correspond more to the interaction flow characteristic: merging two corner streams originating from the passage entrance, which eventually affiliated into a single jet stream [9].

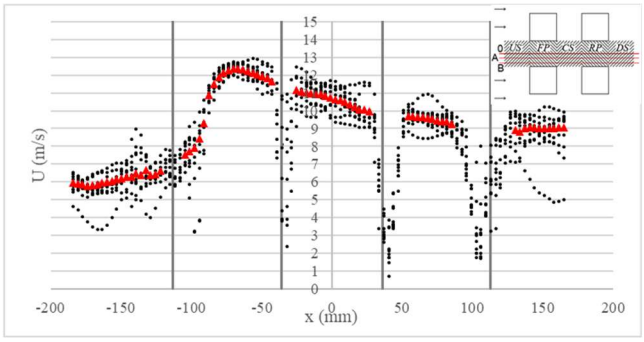


Fig. 8 Experimentation results in centerline

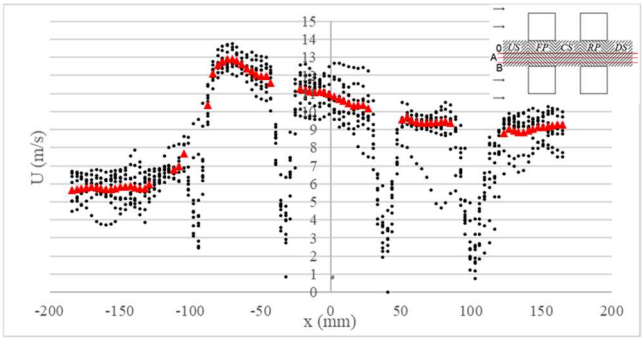


Fig. 9 Experimentation results in Zone-A

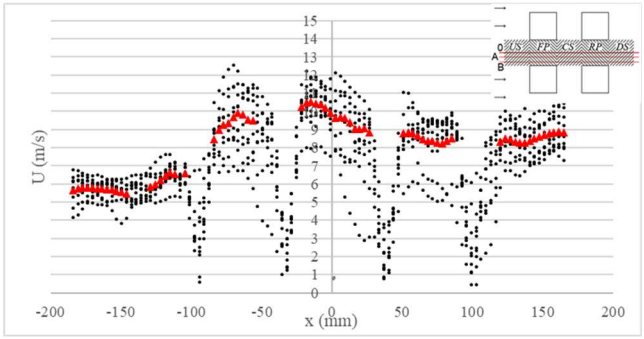


Fig. 10 Experimentation results in Zone-B

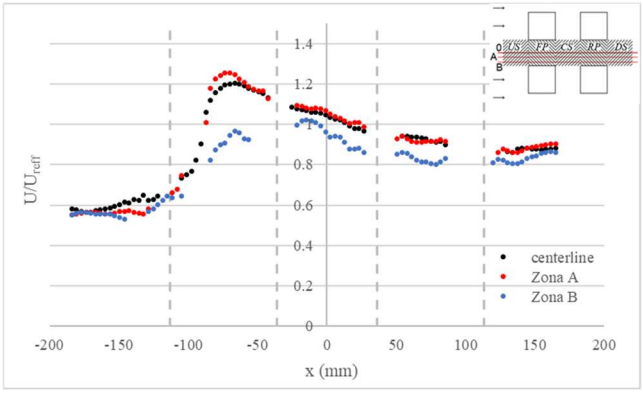


Fig. 11 Wind Speed Amplification for Streamwise data

Fig. 14-16 denote the comparison of the result of wind speed amplification between experimentation and numerical simulation (RANS and LES). At the centerline and zone A, generally, RANS denote better compliance with experimentation compared to LES. Both methods suffice to give wind speed amplification prediction at the front passage well, though RANS tends to underpredict and LES tends to overpredict. Meanwhile, at the cross-stream and rear passage,

the RANS simulation result denotes better compliance than LES. Both numerical simulations offer longitudinal locations of the maximum wind speed amplification at the front passage.

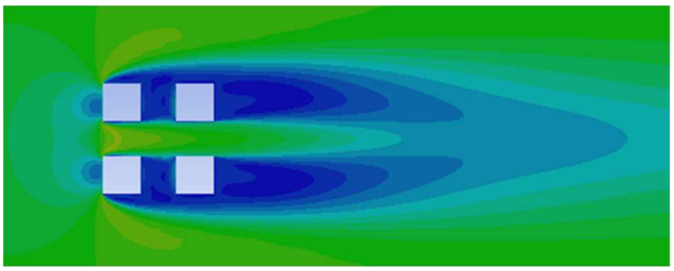

Fig. 12 Wind speed contour (RANS)

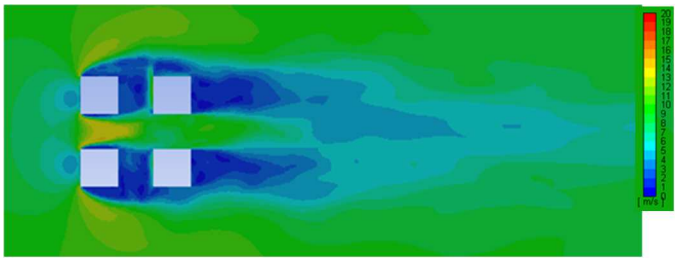

Fig. 13 Wind speed (LES)

In Zone-B (Fig. 16), the results of RANS can be observed: albeit maintaining good suitability of wind speed amplification values, no turbulence field is accounted for, contrasting to the experiment. Meanwhile, the results obtained from LES are sufficient to describe the turbulence field in Zone-B, which is in the shear layer. RANS and LES methods still cannot provide accurate predictions of maximum wind speed amplification due to over-prediction at the front passage location.

In RANS, the highest wind speed amplification value for each zone is 14.9% in the centerline of the zone, 13.4% in Zone A, and 4.7% in Zone B. Ostensibly, the maximum wind speed amplification value is 14.9 % at the zone's center line. This value remains below the prediction given by experimentation, 25.5%, located in zone A. Using the LES method, the wind speed amplification value produced 37.8% in the centerline zone, 40.2% in Zone A, and 24.3% in Zone B. It can be observed that the most considerable maximum wind speed amplification value is 40.2% in Zone A. This indicates that the predicted wind speed amplification value between the two numerical simulation methods is still mismatched; however, LES provided a similar location of the highest wind speed amplification with experimentation. With the highest wind speed amplification value reaching 40.2%, a low-speed wind of 5 m/s may turn into a destructive wind, increasing the damage probability of buildings.

So far, research on the flow around bluff bodies that compares RANS and LES [9] [17] [23] [24] [25], shows that LES always gives better mean wind speed prediction than RANS. However, that research usually focuses on areas where turbulence occurs (corner stream, wake, near-wall), while this study has shown that in the venturi effect, the highest wind speed amplification may be located where turbulence does not dominate (Zone A).

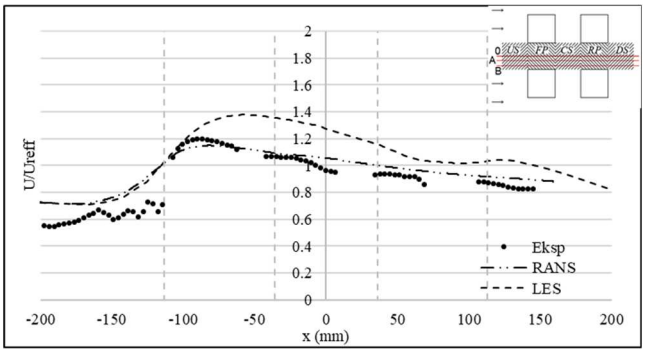


Fig. 14 Wind Speed Amplification Data obtained from the experimentation, RANS-SKE, and LES in the centerline

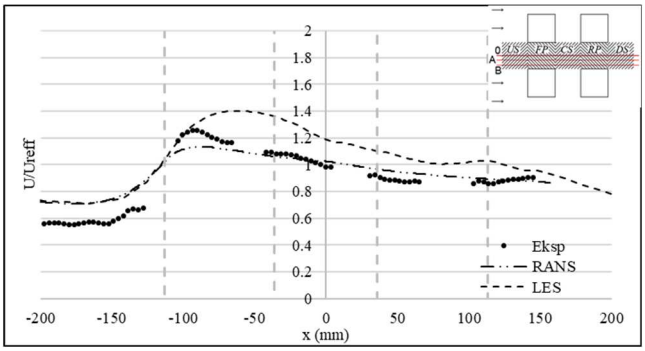


Fig. 15 Wind Speed Amplification Data obtained from the experimentation, RANS-SKE, and LES in Zone-A

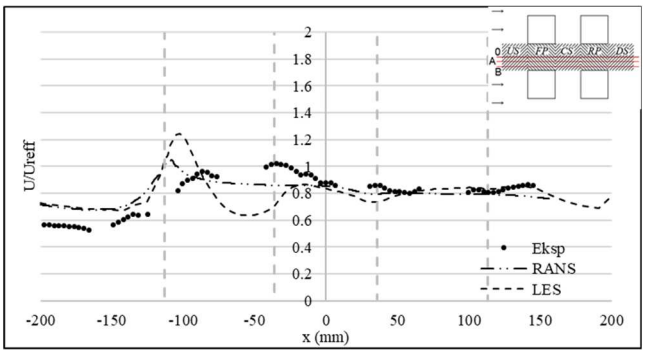


Fig. 16 Wind Speed Amplification Data obtained from the experimentation, RANS-SKE, and LES in Zone-B

### *C. The Effect of Passage Width*

Fig. 17-21 denoted the wind speed contour obtained using the RANS method with several passage width values from 36 mm, 54 mm, 72 mm, 96 mm, and 120 mm, respectively. The left part of the figures shows the wind speed at an elevation of 100 mm, and the right part shows the wind speed at 30 mm. Generally, the wind speed at 30 mm height offers a higher value than wind speed at 100 mm height. It can be concluded that alteration does occur in the wind speed vertical profile from which the buildings exist compared to the upstream location. Such a phenomenon is also likely to happen in the actual condition where the existence of a building may change the vertical profile of the wind flowing through it .

Table IV showed the maximum values of wind speed that occurred in every passage between structures (front passage, cross stream, rear passage), along with wind speed amplification value for RANS method. The maximum wind speed value at a 100 mm elevation is always better for every model. However, the value of wind speed amplification at 30

mm elevation is more excellent. Due to the vertical wind speed profile at the inlet being formed into the power law equation, the greater the elevation, the greater the wind speed value.

Furthermore, Fig. 22- 26 denoted the wind speed contour obtained using the LES method with several passage width values from 36 mm, 54 mm, 72 mm, 96 mm, and 120 mm, respectively. The left part of the figures shows the wind speed at an elevation of 100 mm, and the right part shows the wind speed at 30 mm. The wind speed on the passage has almost a similar pattern to the one generated by the RANS method, which merges two corner streams from each front structure. Nevertheless, at 100 mm elevation, the merging location is way further behind the RANS method. The maximum wind speed amplification value could not be placed on the centerline passage but slightly closer to the structure wall, as found in the experiment. Meanwhile, at 30 mm elevation, both corner streams are not merging into one as shown on every model; this means the flow type that occurred is isolated flow, which signifies that the maximum wind speed amplification location did not take place on the centerline but in the area near the wall.

Table V shows the maximum wind speed that occurred anywhere in the passage (front passage, cross stream, rear passage) along with the wind speed amplification for the LES method. The maximum wind speed value for the RANS method at an elevation of 100 mm is always higher in all the models. Still, at 30mm, the wind speed amplification value at the elevation of 30mm is always higher. Since the inlet velocity profile uses the power law equation, the higher the location, the higher the wind speed. The wind speed amplification value on the LES method tends to be higher at 42.1 % at the elevation of 100 mm and 28.7% at the elevation of 30 mm in the model with $L/S$ = 0.481.

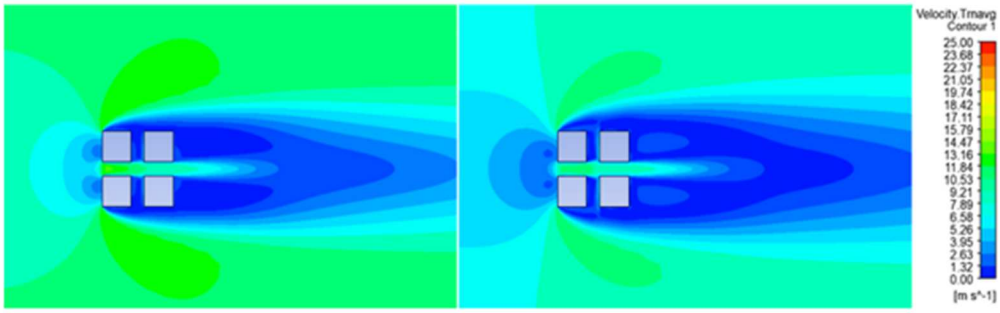


Fig. 17 Wind Speed Contour with Passage Width Variation at The Elevation of 100mm (left) and 30mm (right) with RANS Method for passage width 36 mm; $L/S$ 0.321

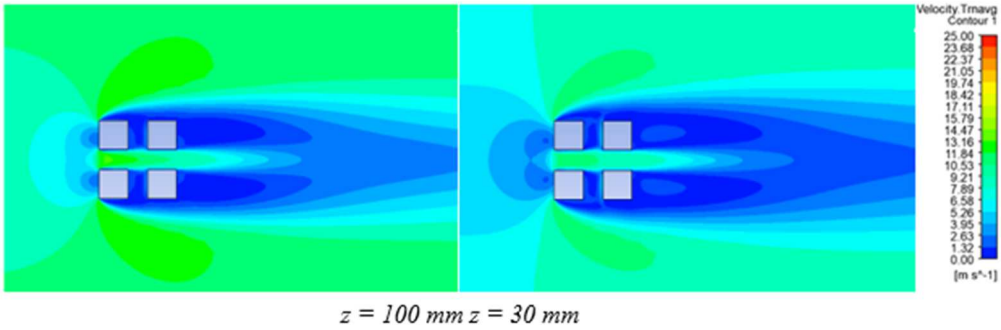


Fig. 18 Wind Speed Contour with Passage Width Variation at The Elevation of 100mm (left) and 30mm (right) with RANS Method for passage width 54 mm; $L/S$ 0.481

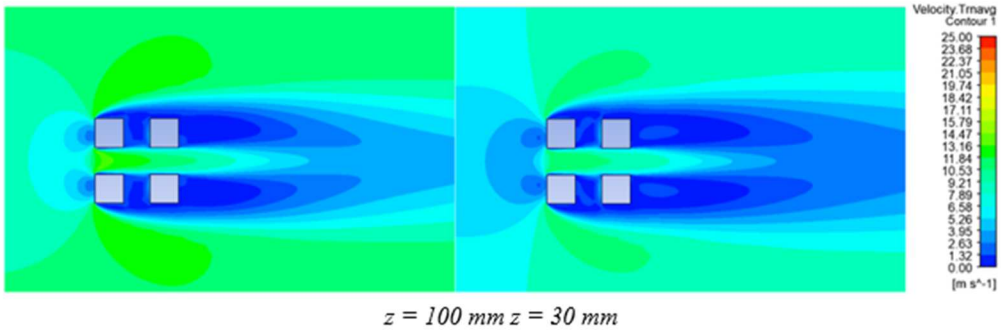


Fig. 19 Wind Speed Contour with Passage Width Variation at The Elevation of 100mm (left) and 30mm (right) with RANS Method for passage width 72 mm; $L/S$ 0.642

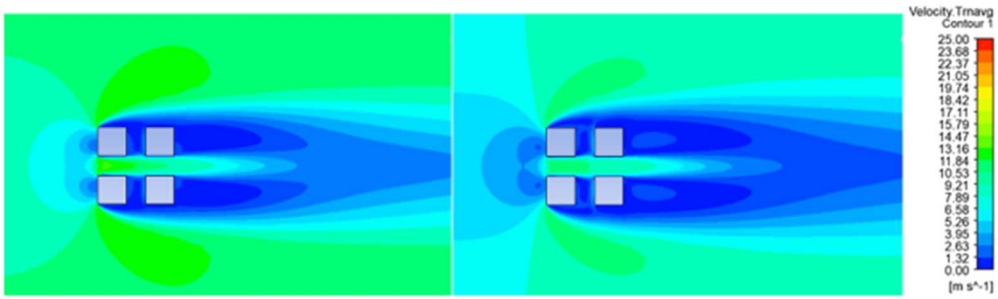


$z = 100\ mm\ z = 30\ mm$

Fig. 20 Wind Speed Contour with Passage Width Variation at The Elevation of 100mm (left) and 30mm (right) with RANS Method for passage width 96 mm; *L/S* 0.856

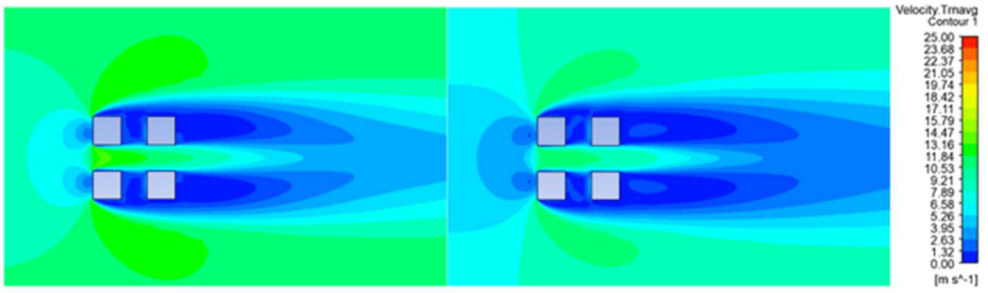


$z = 100\ mm\ z = 30\ mm$

Fig. 21 Wind Speed Contour with Passage Width Variation at The Elevation of 100mm (left) and 30mm (right) with RANS Method for passage width 120 mm; *L/S* 1.070

TABLE IV
PASSAGE WIDTH VARIATION RECAP FOR RANS METHOD

| **RANS** | **Passage width, w(mm)** | **w/S** | **El. 100 mm** | | **El. 30 mm** | |
|---|---|---|---|---|---|---|
| | | | Umax | U/Ureff | Umax | U/Ureff |
| **Model D** | 36 | 0.321 | 12.190 | 1.184 | 9.817 | 1.442 |
| **Model E** | 54 | 0.481 | 12.050 | 1.170 | 10.092 | 1.483 |
| **Model A** | 72 | 0.642 | 11.825 | 1.148 | 10.368 | 1.523 |
| **Model F** | 96 | 0.856 | 11.750 | 1.141 | 10.190 | 1.497 |
| **Model G** | 120 | 1.070 | 11.777 | 1.144 | 10.113 | 1.486 |

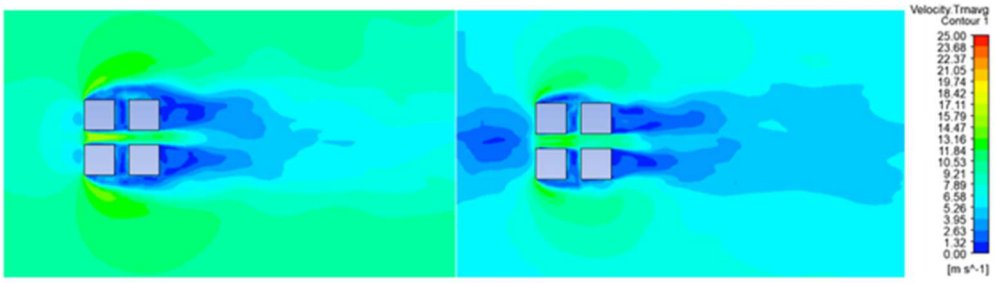


$z = 100\ mm\ z = 30\ mm$

Fig. 22 Wind Speed Contour with Passage Width Variation at The Elevation of 100mm (left) and 30mm (right) with RANS Method for passage width 36 mm; *L/S* 0.321

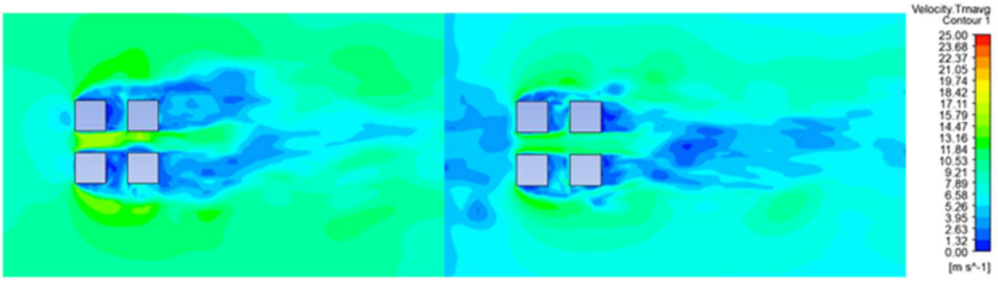


$z = 100\ mm\ z = 30\ mm$

Fig. 23 Wind Speed Contour with Passage Width Variation at The Elevation of 100mm (left) and 30mm (right) with RANS Method for passage width 54 mm; *L/S* 0.481

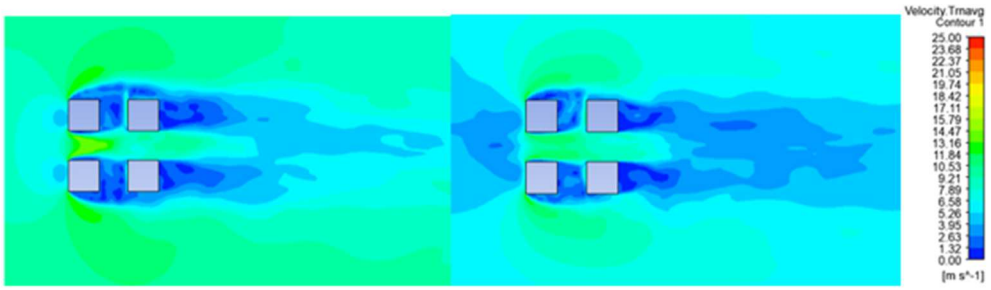


$z = 100\ mm\ z = 30\ mm$

Fig. 24 Wind Speed Contour with Passage Width Variation at The Elevation of 100mm (left) and 30mm (right) with RANS Method for passage width 72 mm; *L/S* 0.642

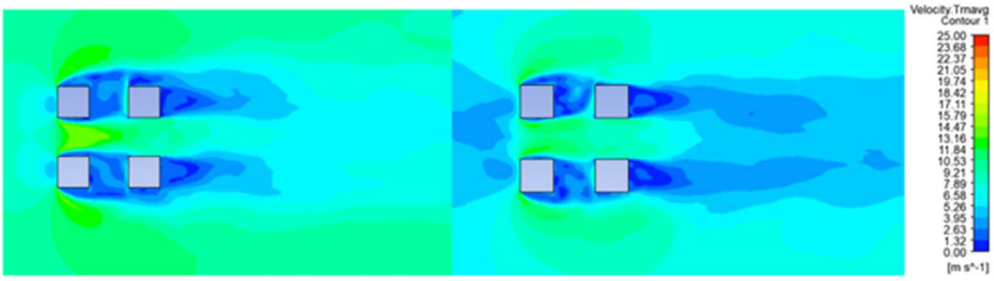


$z = 100\ mm\ z = 30\ mm$

Fig. 25 Wind Speed Contour with Passage Width Variation at The Elevation of 100mm (left) and 30mm (right) with RANS Method for passage width 96 mm; *L/S* 0.856

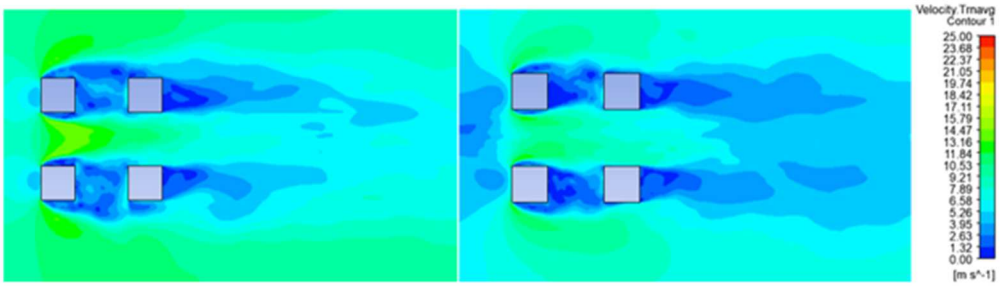


$z = 100\ mm\ z = 30\ mm$

Fig. 26 Wind Speed Contour with Passage Width Variation at The Elevation of 100mm (left) and 30mm (right) with RANS Method for passage width 120 mm; *L/S* 1.070

TABLE V
PASSAGE WIDTH VARIATION RECAP FOR LES METHOD

| **LES** | **Passage width, w (mm)** | **w/S** | **El. 100 mm** | | **El. 30 mm** | |
|---|---|---|---|---|---|---|
| | | | Umax | U/Ureff | Umax | U/Ureff |
| **Model 8** | 36 | 0.321 | 15.527 | 1.510 | 13.082 | 1.925 |
| **Model 9** | 54 | 0.481 | 15.670 | 1.524 | 14.194 | 2.089 |
| **Model 7** | 72 | 0.642 | 15.461 | 1.504 | 14.160 | 2.084 |
| **Model 10** | 96 | 0.856 | 14.327 | 1.394 | 12.766 | 1.878 |
| **Model 11** | 120 | 1.070 | 14.221 | 1.383 | 12.723 | 1.872 |

## IV. CONCLUSION

Numerical simulation of wind flow behavior around high-rise buildings verified by experimental results has been done. The research focuses on the venturi effect in the passage between buildings, represented by the streamwise mean wind speed data. The experimental data processing shows that the highest wind speed amplification is not located at the centerline of the passage. Instead, it is located in Zone A, having a value of 25,5% (at the elevation of 100 mm).

RANS provided the highest wind speed amplification, 14.9%, at the centerline of the passage. Which still lies below the prediction given by experimentation, 25.5%, located in zone A. In contrast, LES results show the highest wind speed amplification, reaching 40.2%, which overpredicts the experimentation results. However, LES provided a similar location of the highest wind speed amplification with experimentation at Zone A. The Passage width that produces the highest wind speed amplification is 54 mm, with the ratio value of the passage width to building influence scale *(L/S)* 0,481. The wind speed at a height of 30 mm is greater than the wind speed measured at 100 mm. This suggests a difference in the vertical profile of wind speed between the location where the buildings exist and the upstream location.

Further research on building model scale should be done to verify CFD accuracy, but such simulation requires a high computational cost. Also different building shapes may give difference windspeed change behaviour around buildings as indicated in the past studies [24] [26] [27] [28] [29] [30] [31].

Moreover, the CFD method is very dependent on the development of computational technology.

## ACKNOWLEDGMENT

We thank the Aerodynamics, Aeroelasticity and Aeroacoustics Laboratory of the Indonesian National Research and Innovation Agency (BRIN) for providing the Wind Tunnel used in this research. This research was funded through the *Program Penelitian, Pengabdian kepada Masyarakat dan Inovasi ITB* (P2MI) administered by Institut Teknologi Bandung.

## REFERENCES

[1] BNPB, (Badan Nasional Penanggulangan Bencana), "Risiko Bencana Indonesia," 2019.

[2] P. Sarli, M. Abdillah and A. Sakti, "Relationship between wind incidents and wind-induced damage to construction in West Java, Indonesia," in *Conf. Ser.: Earth Environ. Sci. 592 012001*, 2020. doi : 10.1088/1755-1315/592/1/012001.

[3] S. Nagar, R. Raj and N. Dev, "Proximity effects between two plus-plan shaped high-rise buildings on mean and RMS pressure coefficients," *Scientia Iranica A,* vol. 29, no. 3, pp. 990-1005, 2022. doi:/10.28991/cej-2021-03091760.

[4] A. Kumar and R. Raj, "Study of Pressure Distribution on an Irregular Octagonal Plan Oval-Shape Building Using CFD," *Civil Engineering Journal,* vol. 7, no. 10, pp. 1787-1805, 2021. doi: 10.28991/cej-2021-03091760.

[5] T. Stathopoulos and R. Storms, "Wind Environmental Conditions in Passages Between Buildings," *Journal of Wind Engineering and Industrial Aerodynamics,* vol. 24, pp. 19-31, 1986. doi: 10.1016/0167-6105(86)90070-X.

[6] B. Blocken, T. Stathopoulos, F. ASCE and J. Carmeliet, "Wind environmental conditions in passages between two long narrow perpendicular buildings," *Journal of Aerospace Engineering,* pp. 280-287, 2008. doi: 10.1016/j.buildenv.2019.106583.

[7] Z. Liu, Z. Yu, X. Chen, R. Cao and F. Zhu, "An investigation on external airflow around low-rise building with various roof types:," *Building and Environment,* vol. 169, 2020. doi:10.1016/j.buildenv.2019.106583.

[8] S. Hassanli, K. Chauhan, M. Zhao and K. C. Kwok, "Application of through-building openings for wind energy harvesting in built environment," *Journal of Wind Engineering and Industrial Aerodynamics,* vol. 184, pp. 445-455, 2019. doi:10.1016/j.jweia.2018.11.030.

[9] B. Blocken, J. Carmeliet and T. Stathopoulos, "CFD evaluation of wind speed conditions in passages between parallel buildings—effect of wall-function roughness modifications for the atmospheric boundary layer flow," *Journal of Wind Engineering and Industrial Aerodynamics,* vol. 95, pp. 941-962, 2007. doi: 10.1088/1757-899X/930/1/012044.

[10] Y. Sanjaya, D. Priambodo, P. W. Sarli and H. D. Setio, "The effect of street canyon width towards wind flow in between high-rise buildings," *4th International Conference on Civil Engineering Research,* vol. 930, 2020. doi: 10.1088/1757-899X/930/1/012044.

[11] D. Priambodo, Y. Sanjaya, P. W. Sarli and H. D. Setio, "Experimental Studies of Wind Flow Inside a Street Canyon Between High-Rise Buildings with Angle of Attack Modifications," *International Journal on Advance Science Engineering Information Technology,* vol. 10, no. 5, pp. 2035-2043, 2020. doi: 10.18517/ijaseit.10.5.12806.

[12] Y. Sanjaya, D. Priambodo and P. W. Sarli, "Pemodelan Numerik Aliran Angin di Sekitar Gedung Tinggi Menggunakan Metode RANS Standard K-E," *Media Komunikasi Teknik Sipil,* vol. 29, no. 1, pp. 153-160, 2022. doi: 10.14710/mkts.v28i1.37375.

[13] H. C. Lim, T. G. Thomas and I. P. Castro, "Flow Around a Cube in a Turbulent Boundary Layer: LES and Experiment," *Journal of Wind Engineering and Industrial Aerodynamics,* vol. 97, pp. 96-109, 2009. oi: 10.1016/j.jweia.2009.01.001.

[14] A. M. Aly and H. Gol-Zaroudi, "Peak pressures on low-rise buildings: CFD LES versus full-scale and wind tunnel measurements," *Wind and Structures,* vol. 30, no. 1, pp. 99-117, 2020. doi:10.1016/j.finmec.2022.100134.

[15] R. Cao, Z. Yu, Z. Liu, X. Chen and F. Zhu, "An investigation of snow drifting on low-sloped gable roofs: Wind-tunnel tests and CFD simulations," *Cold Regions Science and Technology,* vol. 183, no. 103227, 2021. doi:10.1016/j.buildenv.2019.106583.

[16] F.-B. Chen, X.-L. Wang, Y. Zhao, Y.-B. Li, Q.-S. Li, P. Xiang and Y. Li, "Study ofWind Loads and Wind Speed Amplifications on High-Rise Building with Opening by Numerical Simulation and Wind Tunnel Test," *Hindawi Advances in Civil Engineering,* vol. 2020, 2020. doi: 10.1155/2020/8850688.

[17] Y. Abu-Zidan, P. Mendis and T. Gunawardena, "Impact of atmospheric boundary layer inhomogeneity in CFD simulations of tall buildings," *Heliyon,* vol. 6, no. e04274, 2020. doi:10.1016/j.heliyon.2020.e04274.

[18] C. A. Ruiz, I. Kalkman and B. Blocken, "Aerodynamic design optimization of ducted openings through high-rise buildings for wind energy harvesting," *Building and Environment,* vol. 202, no. 108028, 2021. doi: 10.1016/j.buildenv.2021.108028.

[19] Y. Tominaga and M. Shirzadi, "RANS CFD modeling of the flow around a thin windbreak fence with various porosities: Validation using wind tunnel measurements," *Journal of Wind Engineering and Industrial Aerodynamics,* vol. 230, no. 105176, 2022. doi:10.1016/j.jweia.2022.105176.

[20] Y. Abu-Zidan, P. Mendis and T. Gunawardena, "Optimising the computational domain size in CFD simulations of tall buildings," *Heliyon,* vol. 7, no. e06723, 2021. doi : 10.1007/s12273-018-0459-3.

[21] Y. Tominaga, "AIJ guidelines for practical applications of CFD to pedestrian wind environment around buildings," *Journal of Wind Engineering and INdustrial Aerodynamics,* vol. 96, pp. 1749-1761, 2008. doi: 10.1016/j.jweia.2008.02.058.

[22] D. Kasana, D. Tayal, D. Choudhary, R. Raj, R. K. Meena and S. Anbukumar, "Evaluation of aerodynamic effects on a tall building with various cross-section shapes having equal area," *Forces In Mechanics,* vol. 9, no. 100134, 2022. doi:10.1016/j.finmec.2022.100134.

[23] B. Blocken, "LES over RANS in building simulation for outdoor and indoor aplication: A foregone conslusion?," *Building Simulation,* vol. 11, no. 5, pp. 821-870, 2018. doi: 10.1016/j.buildenv.2020.106747.

[24] M. Shirzadi, P. A. Mirzaei and Y. Tominaga1, "CFD analysis of cross-ventilation flow in a group of generic buildings: Comparison between steady RANS, LES and wind tunnel experiments," *BUILD SIMUL,* 2020. doi:10.1016/j.jweia.2022.105176.

[25] X. Zheng, H. Montazeri and B. Blocken, "CFD simulations of wind flow and mean surface pressure for buildings with balconies: Comparison of RANS and LES," *Building And Environment,* vol. 173, no. 106747, 2020. doi: 10.24200/sci.2021.55928.4484.

[26] Y. Li, C. Li, Q.-S. Li, Q. Song, X. Huang and Y.-G. Li, "Aerodynamic performance of CAARC standard tall building model by various corner chamfers," *Journal of Wind Engineering & Industrial Aerodynamics,* vol. 202, no. 104197, 2020. doi:10.1016/J.JWEIA.2020.104197.

[27] N. Gaur and R. Raj, "Aerodynamic mitigation by corner modification on square model under," *Ain Shams Engineering Journal,* 2021. doi:10.1016/j.asej.2021.06.007.

[28] N. Assainar and S. K. Dalui, "Aerodynamic analysis of pentagon-shaped tall buildings," *Asian Journal of Civil Engineering,* 2020. doi: 10.1007/s42107-020-00296-2.

[29] P. Sanyal and S. K. Dalui, "Comparison of aerodynamic coefcients of various types of Y-plan-shaped tall buildings," *Asian Journal of Civil Engineering,* 2020. doi: 10.1007/s42107-020-00265-9.

[30] S. Pal, R. Raj and S. Anbukumar, "Comparative study of wind induced mutual interference effects on square and fish-plan shape tall buildings," *Sadhana,* vol. 46, no. 86, 2021. doi: 10.1007/s12046-021-01592-6.

[31] R. Raj, T. Rana, T. Anchalia and U. Khola, "Numerical Study of Wind Excited Action on H Plan-Shaped Tall Building," *International Journal on Emerging Technologies* , pp. 591-605, 2020. doi:10.28991/CEJ-2022-08-02-06.